THE JOURNAL OF PHYSICAL CHEMISTRY A
A JOURNAL OF THE AMERICAN CHEMICAL SOCIETY

pubs.acs.org/JPCA Article

Solvation of Isoelectronic Halide and Alkali Metal Ions by Argon Atoms

Carly A. Rock, Sarah N. Arradondo, and Gregory S. Tschumper*

Cite This: *J. Phys. Chem. A* 2021, 125, 10524–10531 Read Online

ACCESS | Metrics & More | Article Recommendations | Supporting Information

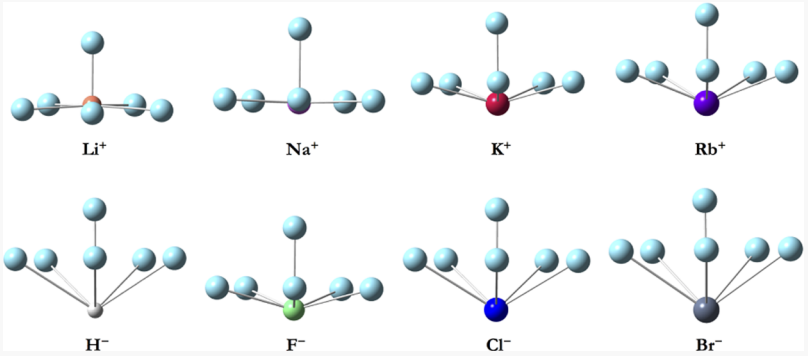

ABSTRACT: This work systematically examines the interactions of alkali metal cations and their isoelectronic halide counterparts with up to six solvating Ar atoms (M^+Ar_n and X^-Ar_n, where M = Li, Na, K, and Rb; X = H, F, Cl, and Br; and n = 1−6) *via* full geometry optimizations with the MP2 method and robust, correlation-consistent quadruple-ζ (QZ) basis sets. 116 unique M^+Ar_n and X^-Ar_n stationary points have been characterized on the MP2/QZ potential energy surface. To the best of our knowledge, approximately two dozen of these stationary points have been reported here for the first time. Some of these new structures are either the lowest-energy stationary point for a particular cluster or energetically competitive with it. The CCSD(T) method was employed to perform additional single-point energy computations upon all MP2/QZ-optimized structures using the same basis set. CCSD(T)/QZ results indicate that internally solvated structures with the ion at/near the geometric center of the cluster have appreciably higher energies than those placing the ion on the periphery. While this study extends the prior investigations of M^+Ar_n clusters found within the literature, it notably provides one of the first thorough characterizations of and comparisons to the corresponding negatively charged X^-Ar_n clusters.

1. INTRODUCTION

The solvation of atomic ions and small charged molecular species plays a vital role in a wide range of critically important phenomena including biochemical processes in our bodies,[1−4] water purification,[5,6] efficient electrochemical reduction of N_2,[7,8] charge transport in fuel cells and batteries,[9,10] and the formation of atmospheric aerosols.[11,12] Small clusters in which a single atomic ion is surrounded by a few uncharged and chemically inert noble gas atoms (Ng = He, Ne, Ar, *etc.*) serve as fundamental prototypes for studying ion solvation. For example, a broad range of experimental and theoretical studies have examined singly charged alkali metal cations in this context (M^+Ng_n, where M = Li, Na, K, *etc.*).[13−55] In contrast, fewer investigations of their isoelectronic halide anion counterparts (X^-Ng_n, where X = H, F, Cl, *etc.*) have been reported, particularly for $n \geq 3$.[56−68]

The clusters formed by sequentially solvating Li^+ or Na^+ with Ar atoms provide the two most thoroughly characterized systems in this family.[21,33,36,39−41,47] Some common low-energy structural motifs have been identified for Li^+Ar_n and Na^+Ar_n clusters in the range of n = 1−6 that resemble the fundamental molecular shapes from the valence-shell electron pair repulsion (VSEPR) theory[69] (*e.g.*, linear, trigonal planar, tetrahedral, trigonal bipyramidal, and octahedral, as depicted by the rightmost entry in each row of Figure 1). Other low-lying structures have also been found that deviate from these highly symmetric configurations, generic examples of which are shown in Figure 1 along with the corresponding point group symmetries (*e.g.*, bent (C_{2v}) rather than linear ($D_{\infty h}$) for n = 2 or square pyramidal (C_{4v}) rather than trigonal bipyramidal (D_{3h}) for n = 5). The different structures identified for a particular cluster often have very similar energies due to the relatively flat nature of the associated potential energy surfaces.

Received: September 13, 2021
Revised: November 16, 2021
Published: December 1, 2021

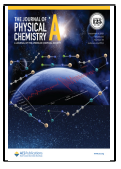

https://doi.org/10.1021/acs.jpca.1c08069
J. Phys. Chem. A 2021, 125, 10524−10531

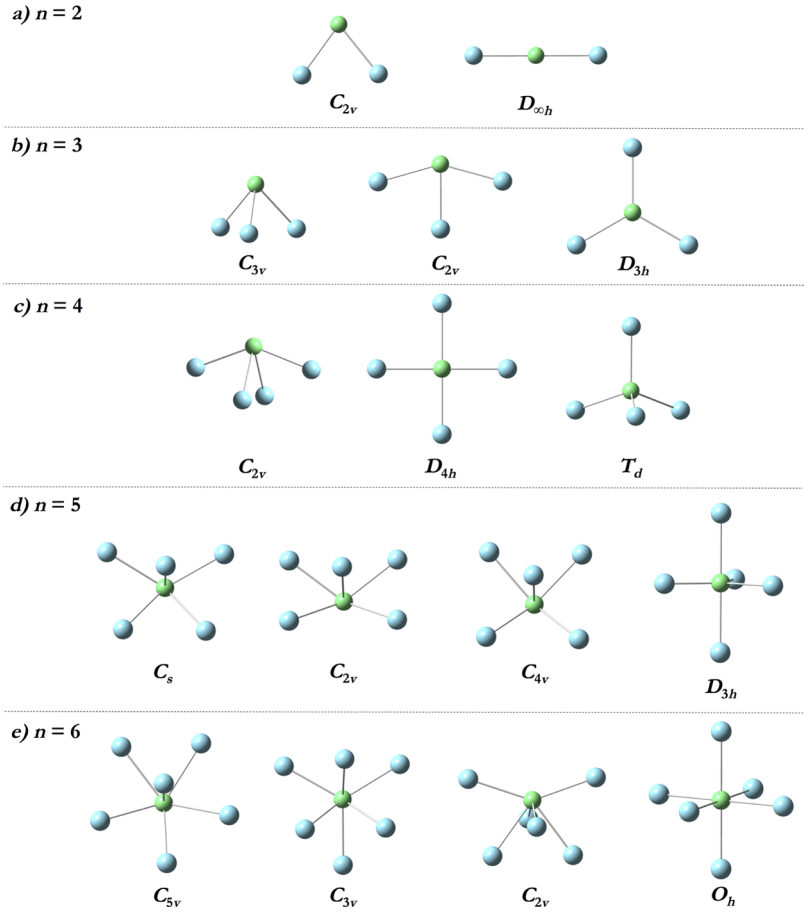

Figure 1. General structures of all configurations and their respective point groups identified for M^+Ar_n and X^-Ar_n clusters.

Consequently, there is still a fair bit of uncertainty regarding the identity of the lowest-energy structures for some of these small clusters where $2 \leq n \leq 6$.

The deceptively challenging characterization of these simple systems is highlighted by a series of MP2 computations on Li^+Ar_2 clusters with various triple- and quadruple-ζ Gaussian atomic orbital basis sets. While some earlier studies have identified the linear $D_{\infty h}$ configuration as the global minimum structure,[41,47] more recent studies have instead concluded that the bent C_{2v} configuration has a lower electronic energy than the linear structure.[21,33] Similar disagreements in the identification of lowest-lying energy structures exist at comparable levels of theory for other cation systems, including Li^+Ar_3 (trigonal planar *vs* pyramidal),[21,33,41,47] Na^+Ar_3 (t-shape *vs* pyramidal *vs* trigonal planar), and Na^+Ar_4 (seesaw *vs* square planar).[36,39,40]

This present study builds upon the prior M^+Ar_n studies by performing a more extensive analysis of the possible structures and energetics of the Li^+Ar_n and Na^+Ar_n systems utilizing the MP2 and CCSD(T) *ab initio* methods and correlation-consistent quadruple-ζ basis sets. This systematic investigation is extended to include the K^+Ar_n and Rb^+Ar_n clusters for n = 1−6, as well as the isoelectronic halide anion counterparts (X^-Ar_n, where X = H, F, Cl, and Br and n = 1−6). This research not only provides some of the first insights into these X^-Ar_n interactions but also compares and contrasts the structures and energetics of isoelectronic M^+Ar_n and X^-Ar_n clusters solvated by up to six Ar atoms.

Finally, we note that although there have been a number of studies examining the related solvated proton systems, the H^+Ng_n clusters are not included in the present study because the solute does not formally have any electrons, which is fundamentally different from the isoelectronic M^+Ng_n and X^-Ng_n clusters that are the focus of the current investigation.

2. COMPUTATIONAL METHODS

Full geometry optimizations were performed upon the M^+Ar_n and X^-Ar_n systems (where M = Li, Na, K, and Rb; X = H, F, Cl, and Br; and n = 1−6) using the second-order Møller−Plesset perturbation theory[70] (MP2) with a series of large correlation-consistent basis sets. These basis sets were augmented with diffuse functions on Ar and X (aug-cc-pV*X*Z),[71−73] whereas weighted core valence correlation-consistent basis sets were used for M (cc-pwCV*X*Z),[74] which include the appropriate pseudopotentials for K and Rb (cc-pwCV*X*Z-PP).[75] Hereafter, all basis sets will be simply denoted as *X*Z, where *X* = T, Q, or 5. Harmonic vibrational frequencies were computed for the lowest-energy optimized structures for each M^+Ar_n and X^-Ar_n cluster at the MP2/QZ level of theory to confirm that they correspond to the minima on the associated potential energy surfaces. The CCSD(T)[76] coupled-cluster method that includes single, double, and a perturbative estimate of connected triple substitutions was employed to perform single-point energy computations upon all MP2/QZ optimized structures with the same basis set. In order to assess the potential effects of the inconsistency commonly referred to as the basis set superposition error (BSSE),[77,78] the Boys−

https://doi.org/10.1021/acs.jpca.1c08069
J. Phys. Chem. A 2021, 125, 10524−10531

Table 1. CCSD(T)/QZ Relative Energies (ΔE) in Kilocalories per Mole for the MP2/QZ Optimized M^+Ar_n and X^-Ar_n Clusters, Where ΔE = 0.00 Represents the Lowest-Energy Configuration for That Particular M^+Ar_n and X^-Ar_n Cluster

n	symmetry	Li^+	Na^+	K^+	Rb^+	H^-	F^-	Cl^-	Br^-
2	C_{2v}	-	+0.01	0.00	0.00	0.00	0.00	0.00	0.00
	$D_{\infty h}$	0.00	0.00	+0.11	+0.17	+0.20	+0.11	+0.18	+0.20
3	C_{3v}	-	0.00	0.00	0.00	0.00	0.00	0.00	0.00
	C_{2v}	-	+0.02	+0.16	+0.21	+0.21	+0.13	+0.20	+0.21
	D_{3h}	0.00	+0.10	+0.39	+0.50	+0.62	+0.33	+0.58	+0.62
4	C_{2v}	-	0.00	0.00	0.00	0.00	0.00	0.00	0.00
	D_{4h}	+1.92	+0.07	+0.40	+0.66	+0.98	+0.34	+0.88	+0.97
	T_d	0.00	+0.10	+0.59	+0.78	+1.03	+0.54	+0.95	+1.02
5	C_s	-	-	0.00	0.00	0.00	0.00	0.00	0.00
	C_{2v}	-	-	+0.04	+0.10	+0.18	+0.05	+0.16	+0.18
	C_{4v}	0.00	0.00	+0.05	+0.13	+0.06	+0.05	+0.27	+0.31
	D_{3h}	+0.05	+0.10	+0.53	+0.86	+1.34	+0.47	+1.23	+1.36
6	C_{5v}	+6.73	+2.29	+0.06	0.00	0.00	+0.14	0.00	0.00
	C_{3v}	-	-	0.00	+0.12	+0.21	0.00	+0.20	+0.19
	C_{2v}	-	-	+0.12	+0.35	+0.56	+0.11	+0.51	+0.54
	O_h	0.00	0.00	+0.43	+1.06	+1.88	+0.33	+1.67	+1.87

Bernardi counterpoise procedure[79,80] (CP) was employed following the protocol detailed elsewhere,[81] using CCSD(T)/QZ single-point energy computations performed upon the MP2/QZ optimized M^+Ar_1 and X^-Ar_1 clusters.

Additional computations were performed with the MP2 and CCSD(T) methods to scan over the interatomic distances in all M^+Ar_1 and X^-Ar_1 clusters using TZ, QZ, and 5Z basis sets. Similarly, relaxed angular scans of the M^+Ar_2 and X^-Ar_2 clusters were performed with the same methods and basis sets. These interatomic distance and relaxed angular scans were performed with the aim to not only compare the electron correlation and basis set effects between the cation and anion systems but also unambiguously identify the global minimum as linear or bent for each M^+Ar_2 and X^-Ar_2 cluster.

Binding energies (E_{bind}) were determined for every structure by comparing the total CCSD(T) energy of each cluster (M^+Ar_n or X^-Ar_n) to those of the isolated fragments (n Ar atoms and either an M^+ ion or an X^- ion). Similarly, the sequential binding energies (E_{bind}^{seq}) for the lowest-energy configurations with n Ar atoms were examined by comparing to the corresponding E_{bind} values for $n - 1$.

All MP2 computations were performed using Gaussian16,[82] and all CCSD(T) computations were performed with Molpro.[83] Analytic Hessians were used to obtain the MP2 harmonic vibrational frequencies. Default frozen-core approximations are often inappropriate for charged systems (especially cations). In this work, all electrons were correlated for H^- and Li^+, whereas the 1s-like orbital was frozen for F^- and Na^+, thereby excluding the two core electrons from the correlation. The 1s-, 2s-, and 2p-like orbitals were frozen for Cl^- and Ar (excluding the 10 core electrons from the correlation), while the 1s-, 2s-, 2p-, 3s-, 3p-, and 3d-like orbitals were frozen for Br^- (excluding the 28 core electrons from the correlation). The 10 core electrons of K were replaced by the 10MDF pseudopotential, and the 28 core electrons of Rb were replaced by the 28MDF pseudopotential, leaving eight electrons for the MP2 and CCSD(T) computations associated with the K^+ and Rb^+ ions.[84]

3. RESULTS AND DISCUSSION

3.1. Geometries and Relative Energies. The MP2 method and QZ basis set were employed for all geometry optimizations after carrying out a series of MP2 and CCSD(T) scans with the TZ, QZ, and 5Z families of basis sets for the n = 1 and 2 clusters. The radial and relaxed angular scans can be found in the Supporting Information along with additional details of this analysis. Structures reported in the previous studies referenced in the Introduction section were used as starting points for identifying the low-energy configurations reported in this work. Figure 1 depicts the general structures and corresponding point-group symmetries of the various stationary points identified within this study. The MP2/QZ optimized Cartesian coordinates for all unique M^+Ar_n and X^-Ar_n stationary points identified in this work are provided in the Supporting Information. The configurations reported here are generally consistent with those reported in the previous literature reports. The structures include the high-symmetry, fundamental geometries familiar to most chemists from the VSEPR theory that effectively place the atomic ions in the geometric center of the solvation shell of Ar atoms (*e.g.*, linear, trigonal planar, tetrahedral, trigonal bipyramidal, and octahedral, as depicted by the rightmost entry in each row of Figure 1), as well as closely related distortions of these basic shapes where the ion is no longer in the geometric center of the solvation shell (bent, pyramidal, t-shaped, seesaw, square pyramidal, *etc.*).

Table 1 reports the CCSD(T)/QZ relative energies (ΔE) for all applicable MP2/QZ optimized M^+Ar_n and X^-Ar_n configurations. MP2/QZ harmonic vibrational frequency computations confirm that there are no imaginary frequencies associated with the lowest-energy structure for each cluster (represented by ΔE = 0.00). A dash in the table (-) indicates that a particular configuration does not correspond to a stationary point for that cluster, a situation only encountered for the two smallest cations (all of the Li^+ clusters and the two largest Na^+ clusters). Apart from these exceptions for Li^+ and Na^+, the MP2/QZ geometry optimizations tend to identify stationary points with the same general structure and point-group symmetry for a given value of n regardless of the identity of the ion (M^+ or X^-).

n = 2: Two stationary points, depicted in Figure 1a, were identified for the n = 2 clusters: linear ($D_{\infty h}$) and bent (C_{2v}). Relaxed angular scans on the MP2 and CCSD(T) potential energy surface with the QZ and 5Z basis sets indicate that the

https://doi.org/10.1021/acs.jpca.1c08069
J. Phys. Chem. A 2021, 125, 10524−10531

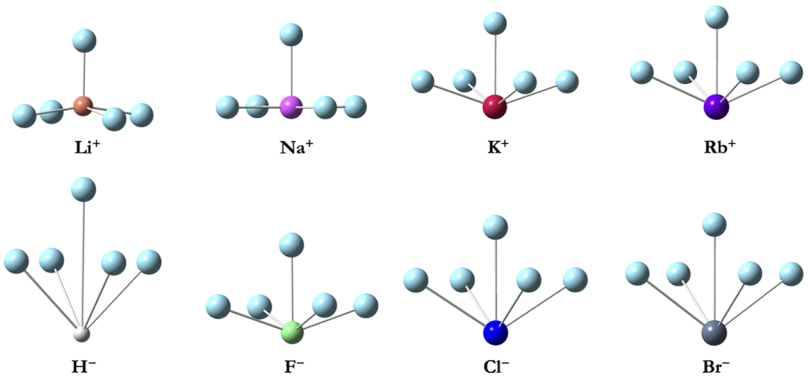

Figure 2. Comparison of the MP2/QZ optimized structures of the C_{4v} M^+Ar_5 and X^-Ar_5 stationary points.

bent stationary point does not exist for Li^+Ar_2 (see the Supporting Information). Structural deviations from the general structures shown in Figure 1 occur for all ions as n is increased up to 6. The simplest case can be described by the unique M^+Ar_2 and X^-Ar_2 C_{2v} configurations, where the angle ranges from 58° for Br^-Ar_2 to 94° for Na^+Ar_2.

As can be seen from the first two rows of the data shown in Table 1, the C_{2v} and $D_{\infty h}$ structures have very similar CCSD(T) energies and are separated by no more than 0.20 kcal mol^{-1}, with the bent stationary points typically having the lower energy. In the case of Na^+, the bent and linear configurations essentially have the same energies with the methods and basis sets employed in this study.

n = 3: Three stationary points, depicted in Figure 1b, were identified for the n = 3 clusters: pyramidal (C_{3v}), t-shaped (C_{2v}), and trigonal planar (D_{3h}). The latter was the only structure identified as a stationary point for Li^+Ar_3 on the MP2/QZ potential energy surface because both the C_{3v} and C_{2v} structures collapse to the higher-symmetry D_{3h} stationary point. The results for n = 3 in Table 1 reveal that the C_{3v} and C_{2v} structures have very similar CCSD(T)/QZ energies and are separated by no more than 0.25 kcal mol^{-1}, with the C_{3v} pyramidal stationary point consistently having the lower energy. The D_{3h} trigonal planar stationary point, on the other hand, is consistently higher in energy with the CCSD(T)/QZ ΔE growing to be as large as 0.62 kcal mol^{-1} for H^-Ar_3.

n = 4: For the clusters containing four solvating Ar atoms, three stationary points were also identified, and they are shown in Figure 1c: seesaw (C_{2v}), square planar (D_{4h}), and tetrahedral (T_d). Once again, a low-symmetry stationary point for the ion with the smallest radius[85] (Li^+) collapses to a higher-symmetry structure when optimized with the MP2 method and QZ basis set (in this case, C_{2v} seesaw → T_d tetrahedral). As seen from the n = 4 data shown in Table 1, the C_{2v} stationary point is consistently the lowest in energy. The square planar and tetrahedral stationary points are noticeably higher in energy (by +0.40 to +1.02 kcal mol^{-1}) than the seesaw stationary point for K^+, Rb^+, H^-, F^-, Cl^-, and Br^-, whereas the corresponding CCSD(T)/QZ ΔE values continue to be smaller for Na^+. In stark contrast, the tetrahedral structure for Li^+Ar_4 is almost 2 kcal mol^{-1} lower in energy than the D_{4h} square planar structure.

n = 5: Four stationary points, depicted in Figure 1d, were identified for the n = 5 clusters: trapezoidal pyramid (C_s), rectangular pyramid (C_{2v}), square pyramid (C_{4v}), and trigonal bipyramid (D_{3h}). Here, the lower-symmetry C_s and C_{2v} stationary points were not identified for the two smallest ions (Li^+ and Na^+). When optimized on the MP2/QZ potential energy surfaces, these structures collapsed to the higher-symmetry (either C_{4v} or D_{3h}) stationary point. The C_s configuration has previously been reported as a stationary point for the H^-Ar_5 cluster by Sebastianelli *et al.*,[60] but this work appears to provide the first analysis of the analogous stationary point for the other X^-Ar_5 and M^+Ar_5 clusters (X = F, Cl, and Br and M = K and Rb). Also, to the best of our knowledge, the C_{2v} rectangular pyramid stationary point has not been previously reported for any of these systems. The n = 5 results in Table 1 show the C_s trapezoidal pyramid to be consistently the lowest in energy for all ions except Li^+ and Na^+. However, the C_s, C_{2v}, and C_{4v} stationary points all have energies within 0.31 kcal mol^{-1} of each other based on CCSD(T)/QZ computations. The D_{3h} trigonal bipyramidal structure tends to have appreciably higher CCSD(T) energies except in the case of Li^+Ar_5 and Na^+Ar_5, for which the ΔE values do not exceed +0.10 kcal mol^{-1}.

One of the most pronounced structural differences between the ions for a particular cluster geometry occurs at n = 5 for the C_{4v} configurations. Figure 2 shows that the ion placement relative to the solvating Ar atoms can differ greatly between the smallest positively and negatively charged ions. In the Li^+Ar_5 cluster on the top left, the Li^+ ion sits 0.4 Å above the plane of Ar atoms that form the base of the square pyramid. The ion position changes significantly for the analogous H^-Ar_5 cluster seen on the bottom left, where the H^- ion sits 2.6 Å below the plane of Ar atoms forming the base of the square pyramid.

n = 6: For the clusters containing six solvating Ar atoms, four stationary points were also identified, and they are depicted in Figure 1e: pentagonal pyramid (C_{5v}), octahedral (O_h), and two distorted structures with C_{3v} and C_{2v} symmetries. As with n = 5, only the two highest-symmetry structures, pentagonal pyramid and octahedral, were identified as stationary points for Li^+Ar_6 and Na^+Ar_6 on the MP2/QZ potential energy surfaces. In comparison to the high-symmetry octahedral stationary point, the C_{5v} and C_{2v} structures appear to both be derived from a pentagonal bipyramid, whereas the C_{3v} structure resembles a distorted trapezoidal bipyramid. Although the C_{5v} pentagonal pyramid has been previously reported as a stationary point for H^-Ar_6[60] and for Rb^+Ar_6[32] and the C_{3v} structure has been previously identified for K^+Ar_6,[43] the corresponding stationary points for all of the other ions have been characterized in this work for the first time to the best of our knowledge. Additionally, it appears that the C_{2v}

https://doi.org/10.1021/acs.jpca.1c08069
J. Phys. Chem. A 2021, 125, 10524−10531

Table 2. CCSD(T)/QZ Binding Energies (E_{bind}) and Sequential Binding Energies (E_{bind}^{seq}) in Kilocalories per Mole for the Lowest-Energy MP2/QZ Optimized M^+Ar_n and X^-Ar_n Clusters

n	Li^+	Na^+	K^+	Rb^+	H^-	F^-	Cl^-	Br^-
				E_{bind}				
1	−6.91	−3.94	−2.54	−2.27	−0.75	−2.48	−1.41	−1.21
2	−13.39	−7.77	−5.14	−4.64	−1.71	−5.01	−3.01	−2.62
3	−19.41	−11.51	−7.85	−7.17	−2.89	−7.61	−4.80	−4.24
4	−24.95	−15.19	−10.52	−9.66	−4.09	−10.19	−6.58	−5.86
5	−28.10	−18.83	−13.18	−12.14	−5.30	−12.75	−8.36	−7.48
6	−32.09	−22.51	−15.82	−14.72	−6.73	−15.30	−10.34	−9.30
				E_{bind}^{seq}				
1[a]	−6.91	−3.94	−2.54	−2.27	−0.75	−2.48	−1.41	−1.21
2	−6.48	−3.83	−2.60	−2.37	−0.96	−2.53	−1.60	−1.41
3	−6.02	−3.74	−2.71	−2.53	−1.18	−2.60	−1.79	−1.62
4	−5.54	−3.68	−2.67	−2.49	−1.20	−2.58	−1.78	−1.62
5	−3.15	−3.64	−2.66	−2.48	−1.21	−2.56	−1.78	−1.62
6	−3.99	−3.68	−2.64	−2.58	−1.43	−2.55	−1.98	−1.82

[a] $E_{bind}^{seq} \equiv E_{bind}$ for $n = 1$.

configuration has yet to be reported as a stationary point for any of the $n = 6$ clusters in this work.

As can be seen in the last four rows of the ΔE data shown in Table 1, the C_{5v} and C_{3v} stationary points compete for the structure with the lowest CCSD(T) energy and are never separated by more than +0.21 kcal mol^{-1}. The C_{3v} structure has the lower energy for K^+ and F^-, whereas the opposite is true for Rb^+, Cl^-, and Br^-. The C_{2v} stationary points identified for K^+ and F^- are also extremely close in energy compared to the corresponding C_{5v} and C_{3v} stationary points, with CCSD(T)/QZ ΔE values not exceeding +0.12 kcal mol^{-1}. The octahedral structure is noticeably higher in energy than the other stationary points for $n = 6$ (with ΔE ranging from +0.43 to +1.88 kcal mol^{-1}). Conversely, the O_h structure is significantly lower in energy (by +6.73 and +2.29 kcal mol^{-1}, respectively) than the C_{5v} structure for Li^+ and Na^+. These large differences in ΔE values are accompanied by significant structural deviations for the unique C_{5v} $n = 6$ configurations. As with $n = 5$, the most pronounced difference occurs between the Li^+ and H^- clusters, where the Li^+ ion prefers to sit 0.1 Å above the plane of Ar atoms that form the base of the pentagonal pyramid and the H^- ion sits 1.9 Å below it. The MP2/QZ optimized Cartesian coordinates for all unique $M^+Ar_{n=5,6}$ and $X^-Ar_{n=5,6}$ stationary points are provided in the Supporting Information.

3.2. Binding Energies. Table 2 reports the CCSD(T)/QZ binding energies (E_{bind}) and corresponding sequential binding energies (E_{bind}^{seq}) for the lowest-energy MP2/QZ optimized M^+Ar_n and X^-Ar_n stationary points reported in this work. E_{bind} values were determined by comparing the total energy of each cluster (M^+Ar_n and X^-Ar_n) to those of the isolated fragments (n Ar atoms and either an M^+ ion or an X^- ion) for $n = 1-6$. E_{bind}^{seq} values were then determined for the lowest-energy stationary point with n Ar atoms by comparing its binding energy to E_{bind} for the corresponding lowest-energy stationary point with one less Ar atom. CCSD(T)/QZ electronic binding energies can be found in the Supporting Information for all unique MP2/QZ optimized M^+Ar_n and X^-Ar_n stationary points identified in this work.

The CCSD(T)/QZ E_{bind} values are located in the upper half of Table 2. The first row of data reveals that Li^+ has the strongest interaction with a single Ar atom (−6.91 kcal mol^{-1}), while H^- has the weakest (−0.75 kcal mol^{-1}) according to CCSD(T)/QZ computations. Moving across the first row of data in the table, the binding strength is inversely proportional to the cation size,[85] decreasing from −6.91 kcal mol^{-1} for Li^+ to −2.27 kcal mol^{-1} for Rb^+. With the exception of H^-, a similar trend is observed for the anions, where the binding energy with a single Ar atom ranges from −2.48 kcal mol^{-1} for F^- to −1.21 kcal mol^{-1} for Br^-. For reference, the binding energy of the Ar dimer is −0.27 kcal mol^{-1} using the same computational protocols, which is consistent with the benchmark values.[86,87]

The CCSD(T)/QZ sequential binding energies, located in the lower half of Table 2, remain fairly consistent as the number of Ar atoms is increased from $n = 2-6$: −3.71 ± 0.11 kcal mol^{-1} for Na^+, −2.66 ± 0.05 kcal mol^{-1} for K^+, −2.49 ± 0.12 kcal mol^{-1} for Rb^+, −1.20 ± 0.24 kcal mol^{-1} for H^-, −2.56 ± 0.05 kcal mol^{-1} for F^-, −1.79 ± 0.19 kcal mol^{-1} for Cl^-, and −1.62 ± 0.21 kcal mol^{-1} for Br^-. The exception to this trend occurs for Li^+Ar_n clusters, where E_{bind}^{seq} values can deviate by almost 2 kcal mol^{-1} from the average (−5.04 ± 1.89 kcal mol^{-1}), whereas analogous deviations for the other ions do not exceed 0.24 kcal mol^{-1}.

In the systems with a single Ar atom, the smallest interatomic distance (R = 2.36 Å) is observed for Li^+Ar which has the largest binding energy for $n = 1$. Moving down that column of the periodic table, R consistently increases to 3.40 Å for Rb^+Ar as the magnitude of the binding energy decreases and the ionic radius increases. The halide ions interacting with one Ar atom exhibit a similar pattern (with the exception of H^-), where Br^-Ar has the largest R value at 3.87 Å. These trends hold as n is increased from 1 to 6. All unique M^+Ar_n and X^-Ar_n R values are reported in the Supporting Information.

The CP procedure was employed to evaluate the significance of the BSSE on the binding energies for the M^+Ar_1 and X^-Ar_1 systems characterized in this work. The CCSD(T)/QZ E_{bind} values computed with the CP procedure (E_{bind}^{CP}) can be found in the Supporting Information. When compared to the data reported in Table 2, the results indicate that the CP procedure decreases the magnitude of the binding energy by 0.12 kcal mol^{-1} for Rb^+Ar_1, by 0.07 kcal mol^{-1} for F^-Ar_1, and by no more than 0.04 kcal mol^{-1} for all of the other ions. These relatively small differences suggest that the CCSD(T)/QZ results presented in this study are close to the complete basis

https://doi.org/10.1021/acs.jpca.1c08069
J. Phys. Chem. A 2021, 125, 10524−10531

set limit, where by definition, the BSSE vanishes. Consequently, the CP procedure was not employed elsewhere in this investigation.

4. CONCLUSIONS

This investigation utilizes *ab initio* methods in conjuction with robust correlation-consistent basis sets to characterize the structures and energetics of singly charged alkali metal cations (M^+) and halide anions (X^-) that are systematically solvated with up to six Ar atoms (M^+Ar_n and X^-Ar_n). As an extension of the previous literature, over 100 unique stationary points were identified for the Li^+Ar_n, Na^+Ar_n, K^+Ar_n, and Rb^+Ar_n systems and their isoelectronic anion counterparts H^-Ar_n, F^-Ar_n, Cl^-Ar_n, and Br^-Ar_n, where n = 1−6. To the best of our knowledge, a significant number of the identified stationary points have been reported here for the first time for several of the M^+Ar_n and X^-Ar_n clusters. These include the C_s and C_{2v} structures for n = 5 and the C_{5v}, C_{3v}, and C_{2v} structures for n = 6. Notably, many of these newly identified structures are either the lowest-energy stationary point for a particular cluster or energetically competitive with it. This work provides one of the first thorough characterizations of the halide family of X^-Ar_n clusters along with comparisons to the corresponding positively charged M^+Ar_n clusters.

The stationary points reported in this work generally have similar structures to those identified in the previous literature reports, but the CCSD(T)/QZ energetics were able to clarify some of the inconsistencies among previously reported lowest-energy stationary points for some of the smaller Li^+ and Na^+ systems. However, more rigorous computational strategies may be required to resolve a few near degeneracies where ΔE is on the order of 0.1 kcal mol^{-1} or less. CCSD(T) geometry optimizations and detailed vibrational analyses of the stationary points would be helpful, but spin−orbit coupling and relativistic effects could also become significant for some of the larger ions (*e.g.*, Rb^+ and Br^-). For a given value of n, MP2/QZ geometry optimizations identify the stationary points with the same general configuration and point-group symmetry for all of the ions present in this work, with the exception of Li^+ and Na^+. As such, the lowest-energy structures are generally in good agreement across the various M^+Ar_n and X^-Ar_n clusters. The internally solvated structures that place the ion at or near the geometric center of the cluster tend to have appreciably higher CCSD(T) energies than those that have the ion near the surface of the cluster, with the exception of Li^+Ar_n.

The CCSD(T)/QZ sequential binding energies for the lowest-energy MP2/QZ optimized M^+Ar_n and X^-Ar_n structures remain fairly consistent for all M^+ and X^- ions except Li^+ as n is increased from 1 to 6. While E_{bind}^{seq} values for Li^+Ar_n become consistently smaller by approximately 0.5 kcal mol^{-1} as the second, third, and fourth Ar atoms are added, the sequential binding energy changes by more than 2 kcal mol^{-1} with the addition of the fifth Ar atom (from −5.54 for n = 4 to −3.15 for n = 5). This large change is consistent with the MP2/6-311G* results previously obtained by Velegrakis and co-workers.[47] Their work revealed an even more significant decrease in E_{bind}^{seq} moving from n = 6 to n = 7, which led to the conclusion that the full primary solvation shell occurs at n = 6 for Li^+Ar_n. A closely related study noted that much larger values of n were required to complete the primary solvation shell for heavier metal cations with larger ionic radii.[50]

ASSOCIATED CONTENT

Supporting Information

The Supporting Information is available free of charge at https://pubs.acs.org/doi/10.1021/acs.jpca.1c08069.

Cartesian coordinates, additional energetic data, and geometrical parameters (PDF)

AUTHOR INFORMATION

Corresponding Author

Gregory S. Tschumper − *Department of Chemistry and Biochemistry, University of Mississippi, University, Mississippi 38677-1848, United States;* orcid.org/0000-0002-3933-2200; Email: tschumpr@olemiss.edu

Authors

Carly A. Rock − *Department of Chemistry and Biochemistry, University of Mississippi, University, Mississippi 38677-1848, United States*

Sarah N. Arradondo − *Department of Chemistry, Washington College, Chestertown, Maryland 21620-1438, United States;* orcid.org/0000-0002-1025-6953

Complete contact information is available at: https://pubs.acs.org/10.1021/acs.jpca.1c08069

Author Contributions

G.S.T. designed and supervised the project. S.N.A. performed the preliminary computations. C.A.R. carried out all computations reported in the results. All authors contributed to the analysis of the data and writing of the manuscript.

Notes

The authors declare no competing financial interest.

ACKNOWLEDGMENTS

This work was supported in part by the National Science Foundation (CHE-166498). The Mississippi Center for Supercomputing Research (MSCR) is also thanked for the generous allocation of time on their computational resources.

REFERENCES

(1) Soozanipour, A.; Sohrabi, H.; Abazar, F.; Khataee, A.; Noorbakhsh, A.; Asadnia, M.; Taheri-Kafrani, A.; Majidi, M. R.; Razmjou, A. Ion Selective Nanochannels: From Critical Principles to Sensing and Biosensing Applications. *Adv. Mater. Technol.* **2021**, *6*, 2000765.

(2) Rosendo-Pineda, M. J.; Moreno, C. M.; Vaca, L. Role of ion channels during cell division. *Cell Calcium* **2020**, *91*, 102258.

(3) Yan, C.; Xue, Z.; Zhao, W.; Wang, J.; Mu, T. Surprising Hofmeister Effects on the Bending Vibration of Water. *ChemPhysChem* **2016**, *17*, 3309−3314.

(4) Gouaux, E.; Mackinnon, R. Principles of Selective Ion Transport in Channels and Pumps. *Science* **2005**, *310*, 1461−1465.

(5) Uliana, A. A.; Bui, N. T.; Kamcev, J.; Taylor, M. K.; Urban, J. J.; Long, J. R. Ion-capture electrodialysis using multifunctional adsorptive membranes. *Science* **2021**, *372*, 296−299.

(6) Porada, S.; Zhao, R.; van der Wal, A.; Presser, V.; Biesheuvel, P. M. Review on the science and technology of water desalination by capacitive deionization. *Prog. Mater. Sci.* **2013**, *58*, 1388−1442.

(7) Westhead, O.; Jervis, R.; Stephens, I. E. L. Is lithium the key for nitrogen electroreduction? *Science* **2021**, *372*, 1149−1150.

(8) Guha, A.; Narayanaru, S.; Kaley, N. M.; Krishna Rao, D.; Mondal, J.; Narayanan, T. N. Mechanistic insight into high yield electrochemical nitrogen reduction using lithium ions. *Mater. Today Commun.* **2019**, *21*, 100700.

(9) Su, X.; Pan, Z.; An, L. Ion Transport Characteristics in Membranes for Direct Formate Fuel Cells. *Fron. Chem.* **2020**, *8*, 765.
(10) Jiang, F.; Peng, P. Elucidating the Performance Limitations of Lithium-ion Batteries due to Species and Charge Transport through Five Characteristic Parameters. *Sci. Rep.* **2016**, *6*, 32639.
(11) Quinn, P. K.; Collins, D. B.; Grassian, V. H.; Prather, K. A.; Bates, T. S. Chemistry and Related Properties of Freshly Emitted Sea Spray Aerosol. *Chem. Rev.* **2015**, *115*, 4383−4399.
(12) Hoppel, W. A.; Gathman, S. G. Charge Transport Through an Aerosol Cloud. *J. Appl. Phys.* **1970**, *41*, 1971−1977.
(13) Jesus, W. S.; Prudente, F. V.; Marques, J. M. C.; Pereira, F. B. Modeling microsolvation clusters with electronic-structure calculations guided by analytical potentials and predictive machine learning techniques. *Phys. Chem. Chem. Phys.* **2021**, *23*, 1738.
(14) Guimarães, M. N.; M. de Almeida, M.; Marques, J. M. C.; Prudente, F. V. A thermodynamic view on the microsolvation of ions by rare gas: application to Li^+ with argon. *Phys. Chem. Chem. Phys.* **2020**, *22*, 10882.
(15) Alharzali, N.; Berriche, H.; Villarreal, P.; Prosmiti, R. Theoretical Study of Cationic Alkali Dimers Interacting with He: Li^{2+}-He and Na^{2+}-He van der Waals Complexes. *J. Phys. Chem. A* **2019**, *123*, 7814−7821.
(16) Ben Hadj Ayed, M.; Osmani, T.; Issaoui, N.; Berisha, A.; Oujia, B.; Ghalla, H. Structures and relative stabilities of Na^+Ne_n (n= 1-16) clusters via pairwise and DFT calculations. *Theor. Chem. Acc.* **2019**, *138*, 84.
(17) Jesus, W. S.; Prudente, F. V.; Marques, J. M. C. Microsolvation of Li^+ in a Mixture of Argon and Krypton: Unveiling the Most Stable Structures of the Clusters. *J. Phys. Chem. A* **2019**, *123*, 2867−2873.
(18) de Tudela, R. P.; Martini, P.; Goulart, M.; Scheier, P.; Pirani, F.; Hernández-Rojas, J.; Bretón, J.; de Zárate, J. O.; Bartolomei, M.; González-Lezana, T.; et al. A combined experimental and theoretical investigation of Cs^+ ions solvated in He_N clusters. *J. Chem. Phys.* **2019**, *150*, 154304.
(19) Jesus, W. S.; Marques, J. M. C.; Prudente, F. V.; Pereira, F. B. Exploring the first-shell and second-shell structures arising in the microsolvation of Li^+ by rare gases. *Int. J. Quantum Chem.* **2018**, *119*, No. e25860.
(20) Rastogi, M.; Leidlmair, C.; An der Lan, L.; Ortiz de Zárate, J.; Pérez de Tudela, R.; Bartolomei, M.; Hernández, M. I.; Campos-Martínez, J.; González-Lezana, T.; Hernández-Rojas, J.; et al. Lithium ions solvated in helium. *Phys. Chem. Chem. Phys.* **2018**, *20*, 25569.
(21) Prudente, F. V.; Marques, J. M. C.; Pereira, F. B. Solvation of Li^+ by argon: how important are three-body forces? *Phys. Chem. Chem. Phys.* **2017**, *19*, 25707.
(22) Slama, M.; Issa, K.; Zbidi, M.; Ben El Hadj Rhouma, M. Microsolvation of K^+ in xenon clusters: a three-body approximation and structural transition. *Mol. Phys.* **2017**, *115*, 757−770.
(23) Slama, M.; Issa, K.; Ben Mohamed, F. E.; Ben El Hadj Rhouma, M.; Spiegelman, F. Structure and stability of Na^+Xe_n clusters. *Eur. Phys. J. D* **2016**, *70*, 242.
(24) Al-Ahmari, M.; Saidi, S.; Dhiflaoui, J.; Hassen, F.; Berriche, H. Structure and Stability of the Li^+Xe_n and $LiXe_n$ Clusters. *J. Cluster Sci.* **2015**, *26*, 913−924.
(25) Issaoui, N.; Abdessalem, K.; Ghalla, H.; Yaghmour, S. J.; Calvo, F.; Oujia, B. Theoretical investigation of the relative stability of Na^+He_n (n= 2-24) clusters: Many-body versus delocalization effects. *J. Chem. Phys.* **2014**, *141*, 174316.
(26) Andrejeva, A.; Gardner, A. M.; Graneek, J. B.; Breckenridge, W. H.; Wright, T. G. Theoretical Study of M^+-RG_2 (M^+ = Li, Na, Be, Mg; RG = He-Rn). *J. Phys. Chem. A* **2013**, *117*, 13578−13590.
(27) Blank, L.; Weeks, D. E.; Kedziora, G. S. M + Ng potential energy curves including spin-orbit coupling for M = K, Rb, Cs and Ng = He, Ne Ar. *J. Chem. Phys.* **2012**, *136*, 124315.
(28) Grandinetti, F. Gas-phase ion chemistry of the noble gases: recent advances and future perspectives. *Eur. J. Mass Spectrom.* **2011**, *17*, 423.
(29) Biring, S. K.; Chaudhury, P. A stochastic optimization method based technique for finding out reaction paths in noble gas clusters perturbed by alkali metal ions. *Chem. Phys.* **2010**, *377*, 46−53.
(30) Tang, L.-Y.; Zhang, J.-Y.; Yan, Z.-C.; Shi, T.-Y.; Mitroy, J. Long-range dispersion coefficients for Li, Li^+, and Be^+ interacting with the rare gases. *J. Chem. Phys.* **2010**, *133*, 104306.
(31) Dhiflaoui, J.; Bouzouita, H.; Berriche, H. Theoretical study of the Na^+Kr_n and $NaKr_n$ (n= 1-25) small clusters. *Phys. Procedia* **2009**, *2*, 1175−1184.
(32) Dhiflaoui, J.; Berriche, H. Stability and structure of the Rb^+Ar_n (n= 1 - 20) small clusters. *Int. J. Nanopart.* **2009**, *2*, 394−401.
(33) Salem, F. B.; Taarit, F.; Hadj Rhouma, M. B. E.; Lakhdar, Z. B. Modélisation classique de champs de forces d'interactions additives dans les agrégats de type X^+ Ar_n, (X = Li et K); mécanisme de croissanceModélisation classique de champs de forces d'interactions additives dans les agrégats de type X+ Arn, (X = Li et K); mécanisme de croissance. *Can. J. Phys.* **2008**, *86*, 911−918.
(34) Breckenridge, W. H.; Ayles, V. L.; Wright, T. G. Analysis of the bonding in alkali-cation/Rg complexes (Rg = He-Xe) using a simple model potential. *Chem. Phys.* **2007**, *333*, 77−84.
(35) Stasikowski, A.; Moneta, M.; Gwizdałła, T. M. The structural properties of alkali metal atoms doped noble gas clusters. *Radiat. Phys. Chem.* **2007**, *76*, 607−611.
(36) Ben El Hadj Rhouma, M.; Calvo, F.; Spiegelman, F. Solvation of Na^+ in Argon Clusters. *J. Phys. Chem. A* **2006**, *110*, 5010−5016.
(37) Di Paola, C.; Sebastianelli, F.; Bodo, E.; Baccarelli, I.; Gianturco, F. A.; Yurtsever, M. Microsolvation of Li^+ in Small He Clusters. Li^+He_n Species from Classical and Quantum Calculations. *J. Chem. Theory Comput.* **2005**, *1*, 1045−1054.
(38) Hickling, H. L.; Viehland, L. A.; Shepherd, D. T.; Soldán, P.; Lee, E. P. F.; Wright, T. G. Spectroscopy of M^+·Rg and transport coefficients of M^+ in Rg (M = Rb-Fr; Rg = He-Rn). *Phys. Chem. Chem. Phys.* **2004**, *6*, 4233−4239.
(39) Giju, K. T.; Roszak, S.; Gora, R. W.; Leszczynski, J. The microsolvation of Na^+: theoretical study of bonding characteristics in weakly bonded Ar_nNa^+ (n= 1-8) clusters. *Chem. Phys. Lett.* **2004**, *391*, 112−119.
(40) Nagata, T.; Aoyagi, M.; Iwata, S. Noble Gas Clusters Doped with a Metal Ion I: Ab Initio Studies of Na^+Ar_n. *J. Phys. Chem. A* **2004**, *108*, 683−690.
(41) Szymczak, J. J.; Giju, K. T.; Roszak, S.; Leszczynski, J. The Li^+ Cation-The Descendant of H^+ or an Ancestor of Na^+? The Properties of Li^+Ar_n (n= 1-6) Clusters. *J. Phys. Chem. A* **2004**, *108*, 6570.
(42) Viehland, L. A.; Lozeille, J.; Soldán, P.; Lee, E. P. F.; Wright, T. G. Spectrscopy of K^+Rg and transport coefficients of K^+ in Rg (Rg = He-Rn). *J. Chem. Phys.* **2004**, *121*, 341.
(43) Hernández-Rojas, J.; Wales, D. J. Global minima for rare gas clusters containing one alkali metal ion. *J. Chem. Phys.* **2003**, *119*, 7800.
(44) Bilalbegovíc, G. Alkali-metal ion in rare gas clusters: global minima. *Phys. Lett. A* **2003**, *308*, 61−66.
(45) Viehland, L. A.; Lozeille, J.; Soldán, P.; Lee, E. P. F.; Wright, T. G. Spectroscopy of Na^+·Rg and transport coefficients of Na^+ in Rg (Rg = He-Rn). *J. Chem. Phys.* **2003**, *119*, 3729.
(46) Lozeille, J.; Winata, E.; Soldán, P.; Lee, E. P. F.; Viehland, L. A.; Wright, T. G. Spectroscopy of Li^+·Rg and Li^+-Rg transport coefficients (Rg = He-Rn). *Phys. Chem. Chem. Phys.* **2002**, *4*, 3601−3610.
(47) Froudakis, G. E.; Farantos, S. C.; Velegrakis, M. Mass spectra and theoretical modeling of Li^+Ne_n, Li^+Ar_n and Li^+Kr_n clusters. *Chem. Phys.* **2000**, *258*, 13−20.
(48) Elford, M. T.; Røeggen, I.; Skullerud, H. R. Interaction potential and transport coefficients for Li^+ ions in helium. *J. Phys. B: At., Mol. Opt. Phys.* **1999**, *32*, 1873−1883.
(49) Prekas, D.; Lüder, C.; Velegrakis, M. Structural transitions in metal ion-doped noble gas clusters: Experiments and molecular dynamics simulations. *J. Chem. Phys.* **1998**, *108*, 4450.
(50) Lüder, C.; Prekas, D.; Velegrakis, M. Ion-Size Effcts in the Growth Sequences of Metal-Ion-Doped Noble Gas Clusters. *Laser Chem.* **1997**, *17*, 109−122.

https://doi.org/10.1021/acs.jpca.1c08069
J. Phys. Chem. A 2021, 125, 10524−10531

(51) Patil, S. H. Adiabatic potentials for alkali-intert gas systems in the ground state. *J. Chem. Phys.* **1991**, *94*, 8089−8095.
(52) Ahlrichs, R.; Böhm, H. J.; Brode, S.; Tang, K. T.; Toennies, J. P. Interaction potentials for alkali ion-rare gas and halogen ion-rare gas systems. *J. Chem. Phys.* **1988**, *88*, 6290.
(53) Pan, R. P.; Etters, R. D. Equilibrium configurations and binding energies for small ionic $Ar_{N-1}K^+$ clusters. *J. Chem. Phys.* **1980**, *72*, 1741.
(54) Nikulin, V. K.; Tsarev, Y. N. On the Calculation of Repulsive Interatomic Interaction Potentials by the Statistical Theory. Pairs of Positive Alkali Metal Ions and Noble Gas Atoms. *Chem. Phys.* **1975**, *10*, 433−437.
(55) Baylis, W. E. Semiempirical, Pseudopotential Calculation of Alkali-Noble-Gas Interatomic Potentials. *J. Chem. Phys.* **1969**, *51*, 2665−2679.
(56) Coccia, E.; Marinetti, F.; Bodo, E.; Gianturco, F. A. Chemical Solution in a Quantum Solvent: Anionic Electrolytes in ^{4}He Nanodroplets. *ChemPhysChem* **2008**, *9*, 1323−1330.
(57) Xinying, L.; Xue, C.; Junhua, J.; Yongfang, Z. Ab initio study of Ar_nI^- (n = 1 − 6) clusters. *Phys. Scr.* **2008**, *78*, 065304.
(58) Wada, A.; Kikkawa, A.; Sugiyama, T.; Hiraoka, K. Thermochemical stabilities of the gas-phase cluster ions of halide ions with rare gas atoms. *Int. J. Mass Spectrom.* **2007**, *267*, 284−287.
(59) Li, X.; Zhao, Y.; Jing, X.; Liu, F.; Hao, F. Ab initio study of Xe_nI^- (n = 1-6) clusters. *Chem. Phys.* **2006**, *328*, 64−68.
(60) Sebastianelli, F.; Baccarelli, I.; Di Paola, C.; Gianturco, F. A. Replacement equivalence of H^- and argon in small $(Ar)_nH^-$ clusters from optimized structure calculations. *J. Chem. Phys.* **2004**, *121*, 2094.
(61) Sebastianelli, F.; Gianturco, F. A. Attachment and Solvation of the H^- Dopant: Structures of Ne_nH^- and Ar_nH^- Clusters from Energy-Optimizing Calculations. *J. Phys. Chem. A* **2004**, *108*, 8633−8640.
(62) Roszak, S.; Leszczynski, J. Ab Initio Studies of the Microsolvation of Ions. *J. Chem. Phys. A* **2003**, *107*, 949.
(63) Sebastianelli, F.; Baccarelli, I.; Di Paola, C.; Gianturco, F. A. Structural and quantum effects from anionic centers in rare gas clusters: The $(Ne)_nH^-$ and $(Ne)_{n+1}$ systems. *J. Chem. Phys.* **2003**, *119*, 5570.
(64) Lenzer, T.; Yourshaw, I.; Furlanetto, M. R.; Pivonka, N. L.; Neumark, D. M. Characterization of $Ar_nCl^{(-)}$ clusters (n = 2-15) using zero electron kinetic energy and partially discriminated threshold photodetachment spectroscopy. *J. Chem. Phys.* **2001**, *115*, 3578.
(65) Pivonka, N. L.; Lenzer, T.; Furlanetto, M. R.; Neumark, D. M. Photoelectron spectroscopy of Xe_nI^- clusters (n ≤ 13). *Chem. Phys. Lett.* **2001**, *334*, 24−30.
(66) Lenzer, T.; Furlanetto, M. R.; Pivonka, N. L.; Neumark, D. M. Zero electron kinetic energy and threshold photodetachment spectroscopy of Xe_nI^- clusters (n = 2-14): Binding, many-body effects, and structures. *J. Chem. Phys.* **1999**, *110*, 6714.
(67) Zeiri, Y. Structure and Dynamics of Cl and Br Ions and Atoms in Xe Clusters. *J. Phys. Chem. A* **1998**, *102*, 2785−2791.
(68) Yourshaw, I.; Zhao, Y.; Neumark, D. M. Many-body effects in weakly bound anion and neutral clusters: Zero electron kinetic energy spectroscopy and threshold photodetachment spectroscopy of Ar_nBr^- (n= 2-9) and Ar_nI^- (n= 2-19). *J. Chem. Phys.* **1996**, *105*, 351.
(69) Gillespie, R. J. The valence-shell electron-pair repulsion (VSEPR) theory of directed valency. *J. Chem. Educ.* **1963**, *40*, 295.
(70) Møller, C.; Plesset, M. S. Note on an Approximation Treatment for Many-electron Systems. *Phys. Rev.* **1934**, *46*, 618−622.
(71) Kendall, R. A.; Dunning, T. H.; Harrison, R. J. Electron affinities of the first-row atoms revisited. Systematic basis sets and wave functions. *J. Chem. Phys.* **1992**, *96*, 6796−6806.
(72) Woon, D. E.; Dunning, T. H. Gaussian Basis Sets for Use in Correlated Molecular Calculations. III. The second row atoms, Al-Ar. *J. Chem. Phys.* **1993**, *98*, 1358.
(73) Wilson, A. K.; Woon, D. E.; Peterson, K. A.; Dunning, T. H. Gaussian basis sets for use in correlated molecular calculations. IX. The atoms gallium through krypton. *J. Chem. Phys.* **1999**, *110*, 7667.
(74) Prascher, B. P.; Woon, D. E.; Peterson, K. A.; Dunning, T. H.; Wilson, A. K. Gaussian basis sets for use in correlated molecular calculations. VII. Valence and core-valence basis sets for Li,Na,Be, and Mg. *Theor. Chem. Acc.* **2011**, *128*, 69.
(75) Hill, J. G.; Peterson, K. A. Gaussian basis sets for use in correlated molecular calculations. XI. Pseudopotential-based and all-electron relativistic basis sets for alkali metal (K-Fr) and alkaline earth (Ca-Ra) elements. *J. Chem. Phys.* **2017**, *147*, 244106.
(76) Purvis, G. D.; Bartlett, R. J. A full coupled-cluster singles and doubles model: The inclusion of disconnected triples. *J. Chem. Phys.* **1982**, *76*, 1910.
(77) Kestner, N. R. He-He Interaction in the SCF-MO Approximation. *J. Chem. Phys.* **1968**, *48*, 252−257.
(78) Liu, B.; McLean, A. D. Accurate calculation of the attractive interaction of two ground state helium atoms. *J. Chem. Phys.* **1973**, *59*, 4557−4558.
(79) Jansen, H. B.; Ros, P. Non-empirical molecular orbital calculations on the protonation of carbon monoxide. *Chem. Phys. Lett.* **1969**, *3*, 140−143.
(80) Boys, S. F.; Bernardi, F. The calculation of small molecular interactions by the differences of separate total energies. Some procedures with reduced errors. *Mol. Phys.* **1970**, *19*, 553−566.
(81) Tschumper, G. S. In *Reviews in Computational Chemistry*; Lipkowitz, K. B., Cundari, T. R., Eds.; Wiley-VCH, Inc.: Hoboken, NJ, 2009; Vol. *26*; Chapter 2, pp 39−90.
(82) Frisch, M. J.; Trucks, G. W.; Schlegel, H. B.; Scuseria, G. E.; Robb, M. A.; Cheeseman, J. R.; Scalmani, G.; Barone, V.; Petersson, G. A.; Nakatsuji, H.; et al. *Gaussian 16*, Revision B.01; Gaussian Inc.: Wallingford CT.2016.
(83) Werner, H.-J.; Knowles, P. J.; Knizia, G.; Manby, F. R.; Schütz, M.; Celani, P.; Györffy, W.; Kats, D.; Korona, T.; Lindh, R.; et al. *MOLPRO*; version 2015.1, a package of ab initio programs.
(84) Lim, I. S.; Schwerdtfeger, P.; Metz, B.; Stoll, H. All-electron and relativistic pseudopotential studies for the group 1 element polarizabilities from K to element 119. *J. Chem. Phys.* **2005**, *122*, 104103.
(85) Rahm, M.; Hoffmann, R.; Ashcroft, N. W. Atomic and Ionic Radii of Elements 1-96. *Chem.—Eur. J.* **2016**, *22*, 14625−14632.
(86) Patkowski, K.; Szalewicz, K. Argon pair potential at basis set and excitation limits. *J. Chem. Phys.* **2010**, *133*, 094304.
(87) Patkowski, K.; Murdachaew, G.; Fou, C.-M.; Szalewicz, K. Accurate ab initio potential for argon dimer including highly repulsive region. *Mol. Phys.* **2005**, *103*, 2031−2045.

https://doi.org/10.1021/acs.jpca.1c08069
J. Phys. Chem. A 2021, 125, 10524−10531